

# Enhanced photocatalytic activity induced by surface plasmon resonance on Ag-loaded strontium titanate nanoparticles

Xu Yan<sup>1</sup>, Shaofang Sun<sup>2</sup>, Bo Hu<sup>1</sup>, Xiyu Wang<sup>1</sup>, Wei Lu<sup>3</sup>, Weidong Shi<sup>1</sup>

<sup>1</sup>School of Chemistry and Chemical Engineering, Jiangsu University, Zhenjiang 212013, People's Republic of China

<sup>2</sup>School of Environmental Science and Engineering, Chang'an University, Xi'an 710054, People's Republic of China

<sup>3</sup>Key Laboratory of Nanodevices and Applications, Suzhou Institute of Nano-Tech and Nano-Bionics, Chinese Academy of Sciences, Suzhou 212013, People's Republic of China

E-mail: swd1978@ujs.edu.cn

Published in Micro & Nano Letters; Received on 23rd July 2013; Accepted on 1st August 2013

Ag nanoparticles-modified cubic-like SrTiO<sub>3</sub> (STO) are fabricated through a classical hydrothermal and photodeposition method. The prepared Ag-STO heterogeneous exhibit an efficient photocatalytic activity (~42% within 1 h reaction time) for degradation of tetracycline under visible-light irradiation, and Ag deposition with 8 mM AgNO<sub>3</sub> exhibited excellent photocatalytic activity. It is considered that this excellent performance results from the surface plasmon resonance of Ag nanoparticles. Meanwhile, the basic principle of the photocatalytic process on the Ag-STO photocatalyst system is also discussed.

**1. Introduction:** Tetracycline (TC), a widely used antibiotic, is usually released into the water environment [1] and directly affects the environment by disrupting the ecosystem equilibrium [2]. Natural bacteria exposed to residual antibiotics, such as TC, could modify their genetic information, develop higher antibiotic resistance and result in multi-resistant strains of micro-organisms [3]. Fortunately, semiconductor-based photocatalysts provide a good tool for the degradation of antibiotics, and much effort has been made to degrade TC by photocatalysis [4, 5].

In recent years, SrTiO<sub>3</sub> (STO) has been considered a promising photocatalyst, and has received much attention [6–10]. However, with the wide bandgap of 3.2 eV, STO cannot make full use of the solar energy [11]. To overcome this fatal defect, many strategies have been employed such as doping with metals, particularly noble metals, non-metallic elements or organic species sensitisation [12–16]. However, the development of more efficient STO-based photocatalyst is necessary for the environment treatment.

The surface plasmon resonance (SPR) is an effective way to enhance the visible-light response of UV-driven semiconductor photocatalysts. Among metal particles that exhibit plasmonic property [17], Ag and Ag/AgX (X = Cl, Br, I) are most reported [18–24]. As the plasmon oscillation occurs, thermal effect and electronic effect are also induced [25]. The SPR effect can sufficiently expand the light absorption of semiconductors into the visible-light region [26–29]. Thus, the enhanced visible-light-driven photocatalytic activity of Ag-STO can be expected. To the best of our knowledge, the SPR effect of Ag-STO is seldom reported but is much desired.

In this reported work, we successfully synthesised Ag-STO nanocomposite photocatalyst. The photocatalytic activity of different samples is measured by the decomposition of TC. The result shows that Ag loading can significantly enhance the photocatalytic activity of STO under visible light. This enhancement can be ascribed to the SPR effect of Ag nanoparticles (NPs). Furthermore, the tentative photocatalytic mechanism of Ag-STO is discussed.

## 2. Experiments

**2.1. Materials and reagents:** Titania TiO<sub>2</sub> (P25) was purchased from Degussa (Germany). The other reference reagents were obtained from Aladdin (China). All chemicals were of analytical grade without further purification and deionised water was used throughout the study.

**2.2. Synthesis of sample:** The cubic STO NPs were prepared by a classical hydrothermal method. In a typical synthesis, 0.847 g Sr(OH)<sub>2</sub> and 0.3 g TiO<sub>2</sub> were mixed in 33.3 ml aqueous solution of 2.1 g KOH, after vigorous stirring for 5 min, and then the mixture solution was transferred to a 50 ml Teflon-lined stainless steel autoclave, and hydrothermally treated in an air-flow electric oven at 150°C for three days. After cooling down naturally, the white precipitate was collected by centrifugation and thoroughly added with deionised water, until a supernatant pH of 7 and then dried at 60°C in air.

During the STO SPR experiment, silver nitrate was chosen as a noble metal source. The Ag-loaded STO (1 mmol) samples were prepared with an extra photodeposition process from a silver nitrate concentration of 2 mmol/l. The photodeposition step was carried out in a 100 ml beaker under the irradiation of two 150 W tungsten halogen lamps for 1 h. Then the product thus obtained was centrifuged, subsequently washed with deionised water and dried at 60°C for 12 h. In parallel, another four samples with different AgNO<sub>3</sub> concentration (4, 6, 8 and 10 mmol/l) were also synthesised by the same procedure as mentioned above.

**2.3. Characterisation:** All of the powder X-ray diffraction (XRD) patterns were obtained on a D/MAX-2500 diffractometer (Rigaku, Japan) using Cu-K $\alpha$  radiation source ( $k = 1.54056$ ) at a scan rate of 5° min<sup>-1</sup> to determine the crystal phase of the obtained samples. The accelerating voltage and the applied current were 50 kV and 300 mA, respectively. Transmission electron microscopy (TEM) and high-resolution TEM (HRTEM) also has been used to characterise the samples. UV-vis diffused reflectance spectra of the samples were collected on a UV-vis spectrophotometer (UV2550, Shimadzu, Japan). BaSO<sub>4</sub> was used as a reflectance standard. Energy dispersive X-ray spectra (EDX) images were collected on an F20 S-TWIN electron microscope (Tecnai G2, FEI Co.), using a 200 kV accelerating voltage.

## 3. Results and discussion

**3.1. Morphology and structure:** The TEM and HRTEM images of the as-prepared Ag-STO products (with 8 mmol/l AgNO<sub>3</sub>) are depicted in Figs. 1a and b, respectively. As shown in Fig. 1a, the cubic STO NPs have a side length of about 50 nm. Obviously, an Ag NP has been adhered to STO NPs, with a size of about 10 nm. Close observation on the nanocomposite is shown in the

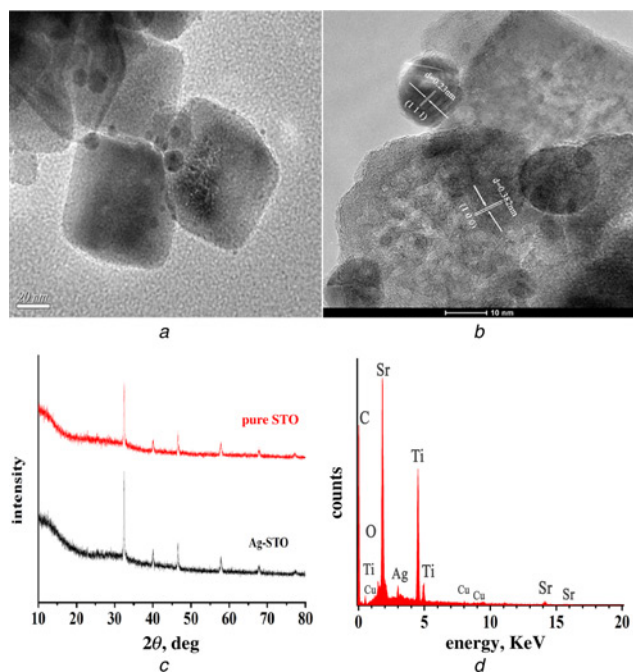


**Figure 1** TEM (Fig. 1a), HRTEM (Fig. 1b), XRD (Fig. 1c) and EDX (Fig. 1d) of prepared Ag-STO (8 mM AgNO<sub>3</sub>)

HRTEM image of Fig. 1b. The characteristic lattice fringe of 0.23 nm corresponds to {1 1 1} diffraction of metallic Ag particles, and the lattice fringe of 0.382 nm is well matched with the {1 0 0} planes of perovskite STO.

The crystalline nature, phase and purity of the as-prepared Ag-STO samples were determined by XRD. As Fig. 1c reveals, the peaks observed at  $2\theta$  values of 22.8°, 32.2°, 40°, 46.5°, 58°, 68° and 77.2° in this pattern are reflections of STO according to the JCPDS Card No. 35-0734. All the diffraction peaks could be indexed as pure STO, and no other diffraction peaks can be observed. The peak with a relative change could be attributed to a different content of silver element. Moreover, no signal about silver can be detected for the low content of the Ag element.

To further confirm the existence of Ag, the areas with the NPs were selected for EDX microanalysis. Fig. 1d depicts the EDX image of the as-prepared Ag-STO (8 mM AgNO<sub>3</sub>) sample, from which Sr, Ti, O and Ag signals can be distinctly observed. It precisely coincides with the elementary composition of SrTiO<sub>3</sub>. The impurity signals of C and Cu are attributed to the carbon-coated supporting copper grid, which is necessary in the STEM-EDX.

Fig 2 is the high-angle annular dark field-scanning transmission electron microscope image of Ag-STO. Corresponding element mapping images indicate the presence of Sr, Ti, O and Ag elements

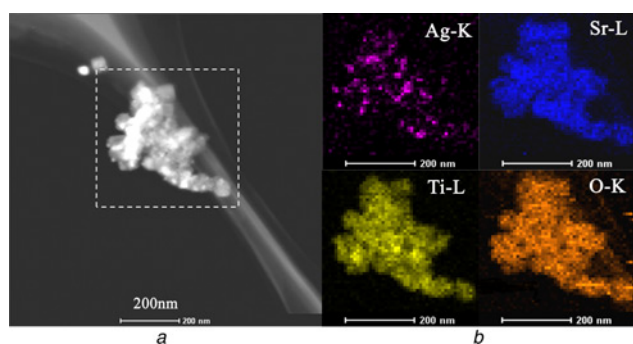


**Figure 2** High-angle annular dark field-scanning transmission electron microscope patterns of Ag-STO (8 mM AgNO<sub>3</sub>)

in single particles (pink dots with size about 10 nm) on the surface of STO NPs, showing the successful combination of Ag NPs with STO NPs, this being consistent with the result of the HRTEM and EDX.

**3.2. UV-vis diffuse reflection spectra:** The UV-vis diffuse reflectance spectrum of different Ag-deposited STO samples compared with the pure STO is shown in Fig. 3. According to the spectrum, the spectra of the Ag-STO samples show a strong broad absorption band between 400 and 800 nm, which covers the entire visible range, and shows a red-shift compared with the spectra of pure STO. An enhancement of the absorption intensity was also observed, and at the absorption peak of 480 nm, this phenomenon is attributed to the plasma resonance effect of the metallic silver NPs.

**3.3. Photocatalytic degradation of TC:** To elucidate the photocatalytic activities of the photocatalysts, the photodegradation of TC experiment was carried out in a photochemical reactor with visible-light irradiation (500 W Xe lamp with a cutoff filter of 400 nm). In each experiment, 100 mg photocatalyst was added into the TC aqueous solution (100 ml, 10 mg/l). Before illumination, the suspensions were magnetically stirred in the dark for 30 min to ensure the establishment of an adsorption-desorption equilibrium between the photocatalyst and TC. The sampling analysis was conducted in 10 min intervals and a 3 ml suspension was sampled and centrifuged to remove the photocatalyst particles. The photocatalytic degradation ratio (DR) was calculated by the following formula

$$DR = (1 - A_i/A_0) \times 100\%$$

$A_0$  is the initial absorbency of TC that reached absorption equilibrium, whereas  $A_i$  is the absorbency after the sampling analysis.

The photocatalytic activity was investigated by degradation TC solution under a visible-light irradiation, and the result is shown in Fig. 4. We note that with the increasing AgNO<sub>3</sub> concentration from 2 to 8 mM, the degradation rate of each Ag-STO sample increased; this is attributed to the success of the SPR of Ag NPs and the generation of electron and hole pair under visible-light irradiation. After 60 min of irradiation, the Ag-STO photocatalyst with 8 mM silver nitrate reached the highest degradation rate of 41.5%. When 10 mM silver nitrate is used in SPR reaction, the photocatalytic activity decreased. It means that too many silver NPs make the charge transfer cost more, and also cause a decrease of photocatalytic activity. The pure STO display a little degradation activity of about 2%, this is because of the photolysis of TC.

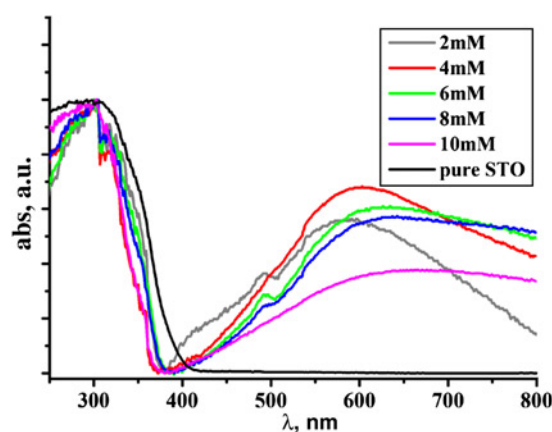


**Figure 3** UV-vis patterns of STO and loaded by different concentration of silver nitrate

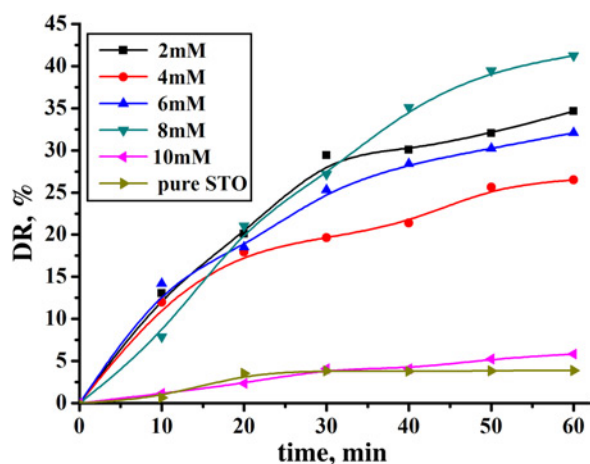


**Figure 4** Photocatalytic activity of Ag-STO with different silver nitrate concentration

This result indicates that Ag loading could significantly raise the visible-light response of UV-light-driven photocatalysts, and too much Ag can lead to a decrease of photocatalytic activity. Further detailed descriptions are given in the following Section.

**3.4. Photocatalytic mechanism:** The tentative photoresponse mechanism might be as follows. (i) The incident photons (visible light) are absorbed by Ag NPs through their SPR excitation, by this collective oscillation, transient local electromagnetic fields are generated by forming electron/hole-rich areas near the surface, and cause a thermal effect as well. (ii) Electrons are injected from the Ag NPs into the conduction band of SrTiO<sub>3</sub>, the holes react with water and generate a •OH. (iii) The electron react with dissolved oxygen of water, and generate  $-O_2^-/O_2^{2-}$ . (iv)  $O_2^-/O_2^{2-}$  can generate more •OH than the degradation of the antibiotic molecule.

When the UV–visible light was utilised as an incident light source, as the light irradiation on the photocatalyst, UV light excited the valance band electron of STO, generated a electron–hole pair, then the electrons ( $e^-$ ) and holes ( $h^+$ ) separated and migrated to the surface of the photocatalyst, the Ag NPs act as an electron trap to reduce the recombination of photoinduced electron–hole pairs and promote interfacial charge transfer. As a result, more photoinduced holes will have the chance to participate in the oxidation reactions on the surface.

Fig. 5 shows a sketch diagram of the basic principle of the photocatalytic process on the Ag-STO photocatalyst system.

In our case, the TC degradation activity is obviously enhanced after the Ag nanoparticle is deposit on the surface of STO. The

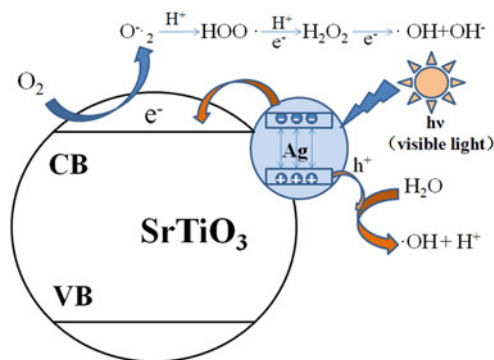


**Figure 5** Possible schematic diagram of the mechanism of the photocatalytic reaction on the Ag-STO photocatalyst system

Ag-STO with 8 mM AgNO<sub>3</sub> exhibits the highest TC DR of 41.5%; this is because of the best photon adsorption, which leads to the increasing of electronic conversion efficiency. However, further increasing the loading amount of Ag will lead to a decrease of the TC DR. The sample prepared with 10 mM AgNO<sub>3</sub> exhibits a lower activity, about 5%. The decreased DR of TC on photocatalysts may be because of the limited light absorption after excess Ag loading. Although absorbing too many Ag NPs on STO causes the photon absorption to increase the contact area between the photocatalyst and TC greatly decrease as well, which means the electrons hardly transfer to the surface of photocatalyst. As a consequence, a suitable Ag-loading amount is crucial for optimising the photocatalytic activity of the cubic Ag-STO nanocrystal photocatalyst.

**4. Conclusion:** In summary, Ag-STO heterojunction plasmonic photocatalyst was fabricated via a facile hydrothermal and photoreduction method. Ag NPs successfully absorbed on the surface of STO NPs. The obtained Ag-STO heterogeneous composites (with 8 mM concentration of silver nitrate solution) exhibited excellent photocatalytic DR (41.5%) of TC under visible-light irradiation, which was ascribed to the SPR caused by the suitable amounts of Ag NPs. All in all, SPR can be a superior strategy to enlarge the light response region of UV photocatalyst; the modified STO photocatalyst has many potential applications for pollutant degradation under visible-light irradiation.

**5. Acknowledgments:** We gratefully acknowledge the financial support of the National Natural Science Foundation of China (grant numbers 21001086, 21276116), the Open Project of the Key Laboratory of Nanodevices and Applications (grant number 13ZS02), the Nature Science Foundation of Jiangsu Province (grant numbers BK2012701, BK2011528), the Postgraduate Research Foundation of Jiangsu Province (grant number 1102123C), the National Postgraduate Research Foundation of China (grant number 2011M500853), the Special Financial Grant from the China Postdoctoral Science Foundation (grant number 2013T60501), the Science Department of Jiangsu Province (grant number BK2010340) and Jiangsu University (grant number 10JDG070).

## 6 References

- [1] Baquero F., Martínez J.L., Cantón R.: 'Antibiotics and antibiotic resistance in water environments', *Curr. Opin. Biotechnol.*, 2008, **19**, pp. 260–265
- [2] Tixier C., Singer H.P., Oellers S., Muller S.R.: 'Occurrence and fate of carbamazepine, clofibric acid, diclofenac, ibuprofen, ketoprofen, and naproxen in surface waters', *Environ. Sci. Technol.*, 2003, **37**, pp. 1061–0
- [3] Bila D.M., Dezotti M.: 'Pharmaceutical drugs in the environment', *Quim. Nova*, 2003, **26**, pp. 523–530
- [4] Kim S., Aga D.S.: 'Potential ecological and human health impacts of antibiotics and antibiotic-resistant bacteria from wastewater treatment plants', *J. Toxicol. Environ. Health. B, Crit. Rev.*, 2007, **10**, pp. 559–573
- [5] Fujishima A., Honda K.: 'Electrochemical photolysis of water at a semiconductor electrode', *Nature*, 1972, **238**, pp. 37–38
- [6] Huo P., Lu Z., Liu X., ET AL.: 'Preparation molecular/ions imprinted photocatalysts of La<sup>3+</sup>@POPD/TiO<sub>2</sub>/fly-ash cenospheres: preferential photodegradation of TCs antibiotics', *Chem. Eng. J.*, 2012, **198–199**, pp. 73–80
- [7] Wang P., Yapa P.S., Lim T.: 'C–N–S tridoped TiO<sub>2</sub> for photocatalytic degradation of tetracycline under visible-light irradiation', *Appl. Catal. A, Gen.*, 2011, **399**, pp. 252–261
- [8] Cardona M.: 'Optical properties and band structure of SrTiO<sub>3</sub> and BaTiO<sub>3</sub>', *Phys. Rev.*, 1965, **140**, p. A651
- [9] Chang C., Shen Y.: 'Synthesis and characterization of chromium doped SrTiO<sub>3</sub> photocatalyst', *Mater. Lett.*, 2006, **60**, pp. 129–132
- [10] Lwashina K., Kudo A.: 'Rh-doped SrTiO<sub>3</sub> photocatalyst electrode showing cathodic photocurrent for water splitting under visible-light irradiation', *J. Am. Chem. Soc.*, 2011, **133**, p. 13272

- [11] Cardona M.: 'Optical properties and band structure of SrTiO<sub>3</sub> and BaTiO<sub>3</sub>', *Phys. Rev.*, 1965, **140**, pp. A651–A655
- [12] Wang J., Yin S., Komatsu M., Sato T.: 'Lanthanum and nitrogen co-doped SrTiO<sub>3</sub> powders as visible light sensitive photocatalyst', *J. Eur. Ceram. Soc.*, 2005, **25**, pp. 3207–3212
- [13] Wang J., Yin S., Komatsu M., Zhang Q., Saito F., Sato T.: 'Photo-oxidation properties of nitrogen doped SrTiO<sub>3</sub> made by mechanical activation', *Appl. Catal. B*, 2004, **52**, pp. 11–21
- [14] Wang D., Ye J., Kako T., Kimura T.: 'Photophysical and photocatalytic properties of SrTiO<sub>3</sub> doped with Cr cations on different sites', *J. Phys. Chem. B*, 2006, **110**, pp. 15824–15830
- [15] Hara S., Irie H.: 'Band structure controls of SrTiO<sub>3</sub> towards two-step overall water splitting', *Appl. Catal. B*, 2012, **115–116**, pp. 330–335
- [16] Zayat Y., Saed A.O., El-Dessouki M.S.: 'Photoelectrochemical properties of dye sensitized Zr-doped SrTiO<sub>3</sub> electrodes', *Int. J. Hydrog. Energy*, 1998, **23**, pp. 259–266
- [17] Kaminskiene Z., Prosycevas I., Stonkute J.: 'Evaluation of optical properties of Ag, Cu, and Co nanoparticles synthesized in organic medium', *Acta Phys. Pol. A*, 2013, **123**, pp. 111–114
- [18] Rycenga M., Cobley C., Zeng J., *ET AL.*: 'Controlling the synthesis and assembly of silver nanostructures for plasmonic applications', *Chem. Rev.*, 2011, **111**, pp. 3669–3712
- [19] Liang S., Liu X., Yang Y., *ET AL.*: 'Symmetric and asymmetric Au – AgCdSe hybrid nanorods', *Nano Lett.*, 2012, **12**, pp. 5281–5286
- [20] Li J., Cushing S.K., Bright J., *ET AL.*: 'Ag@Cu<sub>2</sub>O core-shell nanoparticles as visible-light plasmonic photocatalysts', *ACS Catal.*, 2013, **3**, pp. 47–51
- [21] Sankar S., Gopchandran K.G.: 'Rutile TiO<sub>2</sub> (101) based plasmonic nanostructures', *Ceram. Int.*, 2013, **39**, pp. 1081–1086
- [22] Chen K., Pu Y., Chang K., *ET AL.*: 'Ag-nanoparticle-decorated SiO<sub>2</sub> nanospheres exhibiting remarkable plasmon-mediated photocatalytic properties', *J. Phys. Chem. C*, 2012, **116**, pp. 19039–19045
- [23] Pyne S., Sahoo G.P., Bhui D.K., *ET AL.*: 'Enhanced photocatalytic activity of metal coated ZnO nanowires', *Spectrochim. Acta A*, 2012, **93**, pp. 100–105
- [24] Hou J., Wang Z., Yang C., Zhou W., Jiao S., Zhu H.: 'Hierarchically plasmonic Z-scheme photocatalyst of Ag/AgCl nanocrystals decorated mesoporous single-crystalline metastable Bi<sub>20</sub>TiO<sub>32</sub> nanosheets', *J. Phys. Chem. C*, 2013, **117**, pp. 5132–5141
- [25] Zhou X., Liu G., Yu J., Fan W.: 'Surface plasmon resonance-mediated photocatalysis by noble metal-based composites under visible light', *J. Mater. Chem.*, 2012, **22**, pp. 21337–21354
- [26] Wang X., Kong X.G., Yu Y., Sun Y.J., Zhang H.: 'Effect of annealing on upconversion luminescence of ZnO: Er<sup>3+</sup> nanocrystals and high thermal sensitivity', *J. Phys. Chem. C*, 2007, **111**, pp. 15119–15124
- [27] Ma G.H., He J., Rajiv K., Tang S.H., Yang Y., Nogami M.: 'Observation of resonant energy transfer in Au: CdS nanocomposite', *Appl. Phys. Lett.*, 2004, **84**, pp. 4684–4686
- [28] Lin H., Chen Y., Wu J.G., Wang D.I., Chen C.: 'Carrier transfer induced photoluminescence change in metal-semiconductor core-shell nanostructures', *Appl. Phys. Lett.*, 2006, **88**, p. 161911
- [29] Mishra Y.K., Mohapatra S., Singhal R., Avasthi D.K., Agarwal D.C., Ogale S.B.: 'Au-ZnO; a tunable localized surface plasmonic nanocomposite', *Appl. Phys. Lett.*, 2008, **92**, article id 043107